Journal of Mathematical Biology (2022) 85:50
https://doi.org/10.1007/s00285-022-01825-0

Mathematical Biology

Spatial dynamics of a vegetation model with uptake–diffusion feedback in an arid environment

Gui-Quan Sun[1,2] · Li-Feng Hou[2] · Li Li[3,4] · Zhen Jin[2] · Hao Wang[5]

Received: 6 July 2021 / Revised: 20 September 2022 / Accepted: 3 October 2022

Abstract
Vegetation patterns with a variety of structures is amazing phenomena in arid or semi-arid areas, which can identify the evolution law of vegetation and are typical signals of ecosystem functions. Many achievements have been made in this respect, yet the mechanisms of uptake–diffusion feedback on the pattern structures of vegetation is not fully understood. To well reveal the influences of parameters perturbation on the pattern formation of vegetation, we give a comprehensive analysis on a vegetation–water model in the forms of reaction–diffusion equation which is posed by Zelnik et al. (Proc Natl Acad Sci 112:12,327–12,331, 2015). We obtain the exact parameters range for stationary patterns and show the dynamical behaviors near the bifurcation point based on nonlinear analysis. It is found that the model has the properties of spot, labyrinth and gap patterns. Moreover, water diffusion rate prohibits the growth of vegetation while shading parameter promotes the increase of vegetation biomass. Our results show that gradual transitions from uniform state to gap pattern can occur for suitable value of parameters which may induce the emergence of desertification.

Keywords Vegetation model · Turing pattern · Multi-scale analysis · Uptake–diffusion feedback · Shading effect · Regime shifts

Mathematics Subject Classification 35B36 · 35B38 · 35Q92 · 92D25 · 92D40

✉ Hao Wang
hao8@ualberta.ca

1 Department of Mathematics, North University of China, Taiyuan 030051, Shanxi, China

2 Complex Systems Research Center, Shanxi University, Taiyuan 030006, Shanxi, China

3 School of Computer and Information Technology, Shanxi University, Taiyuan 030006, Shanxi, China

4 Science and Technology on Electronic Test and Measurement Laboratory, North University of China, Taiyuan 030051, Shanxi, China

5 Department of Mathematical and Statistical Sciences, University of Alberta, Edmonton T6G 2G1, Canada

Published online: 13 October 2022

1 Introduction

Vegetation is the foundation for the existence and development of the ecosystem, and determines the structure and function of ecosystem to a great extent, which is thus considered as the engineers of ecosystem (Jones et al. 1994; Gilad et al. 2004). In addition, vegetation can absorb carbon dioxide and produce oxygen through photosynthesis, thereby purifying the air and improving the environment (Lemordant et al. 2018; Gallagher et al. 2019). The roots of vegetation can protect slope land and conserve water. The leaves of vegetation can perform transpiration, reduce land drought and prevent land desertification.

Desertification has always been the focus of people's attention, especially in the arid and semi-arid areas where the ecological environment is very fragile, and desertification phenomenon is particularly serious. At present, we have observed various pattern structures in arid and semi-arid regions all over the world, such as spot pattern, strip (labyrinth) pattern and gap pattern (von Hardenberg et al. 2001; Rietkerk et al. 2002, 2004; Garfinkel et al. 2004; Rietkerk and Van de Koppel 2008; Borgogno et al. 2009). Many experts and scholars have also established a series of mathematical models to study them (Gilad et al. 2004, 2007; Klausmeier 1999; HilleRisLambers et al. 2001; Meron et al. 2004; Sherratt and Synodinos 2012; Sun et al. 2018, 2022). Typically in 1999, Klausmeier constructed a mathematical model with vegetation biomass and water density as variables based on the assumptions of ecological reality, which was the earlier model to study the dynamical relationship between vegetation and water. It captures regular and irregular patterns in semi-arid areas and explains the importance of nonlinear mechanisms in determining the spatial structure of plant communities (Klausmeier 1999). In 2002, Rietkerk et al. divided water into soil water and surface water, and posed a spatial model to study the positive feedback between plant density and water infiltration, as well as the influence of spatial distribution of runoff water on the formation of vegetation pattern (HilleRisLambers et al. 2001). In 2007, Gilad et al. proposed a mathematical model to study dryland ecosystem engineering. The model captures various feedback mechanisms between biomass and water, studied biomass patterns along drought gradients, and found that there is a trade-off between the engineering ability of plant species and their ability to recover from disturbances (Gilad et al. 2007). In 2015, Zelnik et al. simplified the model proposed by Gilad et al., and used such model and empirical data to study the dynamics of the fairy circle ecosystem in Zelnik et al. (2015).

It is well known that precipitation is the main source of water needed for vegetation growth, and vegetation can absorb this water through two ways. Firstly, it is directly absorbed by the leaves. Secondly, the vegetation absorbs the water that penetrates into the soil through the roots. Obviously, the water absorbed by the vegetation through the leaves has little effect on the growth of the vegetation, and the growth of vegetation depends mainly on the absorption of water by the roots. In this process, there is a positive feedback between vegetation growth and water transport to growing vegetation, and the pattern formation is driven by this positive feedback mechanism (Meron 2012). At present, the water transport mechanism can be divided into at leastthree

types (Kinast et al. 2014): Infiltration feedback, and the infiltration ability of water is stronger in the area with higher vegetation biomass. The root-augmentation feedback, with the growth of plants, the root zone of vegetation extends to a new area, where the roots can continue to absorb water and further promote the growth of vegetation (Gilad et al. 2007; Meron 2011). The uptake–diffusion feedback, the higher biomass vegetation can increase the water absorption rate and reduce the soil water density nearby, which leads to the rapid transportation of soil water from the sparse vegetation area to the densely vegetated area, that is to say, the area with high soil water density is transported to the area with low soil water density (Kinast et al. 2014; Zelnik et al. 2016). This mechanism requires a large soil water diffusivity in dryland ecosystems, and a non-linear relationship between plant water absorption rate and biomass. Previous studies have shown that the ecosystem of Namibian fairy circle is a good embodiment of this mechanism (Zelnik et al. 2015).

Vegetation pattern is a kind of spatial self-organizing phenomenon (Rietkerk et al. 2002, 2004; Barbier et al. 2006; Li et al. 2022a, b), which can be explained by three deterministic models: Turing model, kernel based model, and differential flow model. Although these models are different in mathematical descriptions, the pattern formation mechanisms behind them are similar, that is, the instability of symmetry breaking. In the first two models, this symmetry breaking is caused by the interaction between short-range facilitation and long-range inhibition. In the differential flow model, the symmetry breaking is caused by the velocity difference between different species (Borgogno et al. 2009; Turing 1952; Cross and Greenside 2009).

It should be noted that model parameters play important role on pattern dynamics of vegetation (Kéfi et al. 2007; Sherratt 2005; Sherratt and Lord 2007; Sherratt 2015). As a result, we give a rounded analysis on the effects of the uptake–diffusion feedback and shading on vegetation patterns in a vegetation model posed by Zelnik et al. (2015). The rest of this work is as follows. In Sect. 2, we study the existence and stability on equilibrium points of a vegetation-water model, and derive the conditions for producing Turing patterns. In Sect. 3, we use the multi-scale analysis method to derive the amplitude equation based on nonlinear analysis. In Sect. 4, we show the influences of water diffusion and shading on vegetation growth from the aspect of pattern structures and biomass change. Conclusions and discussions are given in the last section.

2 Mathematical model and analysis

2.1 Model formulation

In arid and semi-arid areas, rainfall is the main water source for vegetation growth. After the rainfall reaches the ground, one part of the rainfall penetrates into the soil and becomes groundwater or surface runoff, and the other part is lost to the atmosphere through transpiration of vegetation and evaporation of the ground. As we all know, the root system is the main organ of terrestrial vegetation absorbing water, it will absorb a lot of water from the soil to supply the growth and development of vegetation. Due

to the large amount of water absorbed by the roots of the vegetation, the soil water concentration at this location decreases, resulting in a concentration difference with the surrounding soil water concentration, which in turn causes the soil water diffusion (Fig. 1).

The interaction between vegetation and water is carried out through various feedback mechanisms. In 2007, Gilad et al. proposed a single plant species model in limited water resources, which captures three kinds of feedback of pattern formation, including infiltration feedback, root augmentation feedback and uptake–diffusion feedback. The model consists of three variables: vegetation biomass $B(X, T)$, soil–water $W(X, T)$ and surface water $H(X, T)$, as follows (Gilad et al. 2007):

$$\begin{cases} B_T = G_B B(1 - B/K) - MB + D_B \nabla^2 B, \\ W_T = IH - N(1 - RB/K)W - G_W W + D_W \nabla^2 W, \\ H_T = P - IH + D_H \nabla^2 (H^2), \end{cases} \tag{2.1}$$

where G_B is the growth rate of biomass and G_W is the water absorption rate, with the following forms:

$$\begin{aligned} G_B(X, T) &= \Lambda \int_\Omega G(X, X', T) W(X', T) dX', \\ G_W(X, T) &= \Gamma \int_\Omega G(X', X, T) B(X', T) dX', \\ G(X, X', T) &= \frac{1}{2\pi S_0^2} \exp[-\frac{|X - X'|^2}{2S_0^2(1 + EB(X, T))^2}], \end{aligned}$$

and

$$I = A \frac{B(X, T) + Qf}{B(X, T) + Q}.$$

To simplify the model, we make the following assumptions. Firstly, we assume that the distribution of kernel function $G(X, X', T)$ is very narrow (i.e. $S_0 \longrightarrow 0$), then one can use Dirac delta function approximation (Zelnik et al. 2015; Meron 2018), i.e.

$$\begin{aligned} &\lim_{S_0 \to 0} G(X, X', T) \\ &= (1 + EB(X, T))^2 \lim_{S_0 \to 0} \frac{1}{2\pi S_0^2 (1 + EB(X, T))^2} \exp\left[-\frac{|X - X'|^2}{2S_0^2(1 + EB(X, T))^2} \right] \\ &= (1 + EB(X, T))^2 \delta(X - X'). \end{aligned} \tag{2.2}$$

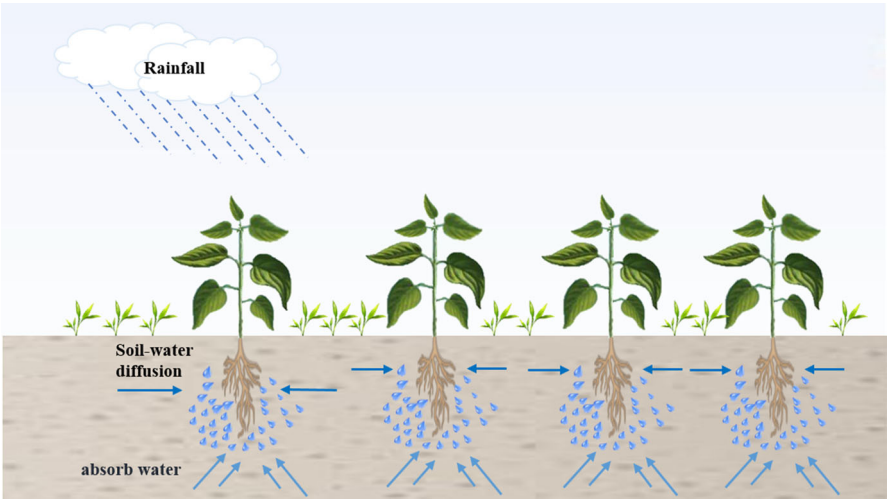

Fig. 1 Schematic diagram of soil–water diffusion feedback. Soil–water is absorbed by the roots of vegetation, resulting in the concentration difference, which leads to the directional flow of water

Taking (2.2) into the expressions of G_B and G_W, and then according to the "screening" nature of the δ function, one can have:

$$\begin{aligned} G_B(X,T) &= \Lambda(1+EB(X,T))^2 \int_\Omega \delta(X-X')W(X',T)dX' \\ &= \Lambda(1+EB(X,T))^2 \int_\Omega \delta(X'-X)W(X',T)dX' \\ &= \Lambda(1+EB(X,T))^2 W(X,T). \end{aligned} \tag{2.3}$$

In the same way, we can get:

$$G_W = \Gamma B(1+EB)^2. \tag{2.4}$$

Secondly, we assume that the infiltration rate I of bare land is the same as that of vegetation covered area (i.e. $f = 1$), then $I = A$ is constant, and thus the surface water (H) equation is independent, which has a linear stable uniform solution, $H_0 = P/I$. Obviously, H is a fast variable, while B and W are slow variables. Therefore, we can assume that H has reached the stable state H_0 in the change of B and W (i.e. $H = H_0$) and combining with formula (2.3) and (2.4), we can get the following two variables model:

$$\begin{cases} \partial_T B = \Lambda W B\left(1-\dfrac{B}{K}\right)(1+EB)^2 - MB + D_B\nabla^2 B, \\ \partial_T W = P - N\left(1-\dfrac{RB}{K}\right)W - \Gamma W B(1+EB)^2 + D_W\nabla^2 W, \end{cases} \tag{2.5}$$

where $\nabla^2 = \partial^2_X + \partial^2_Y$. B(X,T) is vegetation biomass and W(X,T) is soil–water density. In the first equation, Λ is conversion coefficient of vegetation growth from water absorption, K describes the maximum standing biomass, E provides a measure for the root-to-shoot ratio, M is the rate of plant loss due to mortality or grazing. In the second equation, P is precipitation rate, N represents water evaporation rate, R represents the decrease in soil water evaporation rate due to shading, and Γ represents the water consumption rate due to water absorption by vegetation (see Table 1). We can find that only one feedback mechanism is captured in model (2.5), that is, the uptake–diffusion feedback. The uptake–diffusion feedback can be reflected by the soil–water loss term $-\Gamma W B(1+EB)^2$ and the diffusion term $D_W \nabla^2 W$ (Kinast et al. 2014; Zelnik et al. 2016; Meron 2018).

For the convenience of later analysis, we need to make the model dimensionless, so we make the following variable substitution (Zelnik et al. 2015):

$$b = \frac{B}{K}; w = \frac{W\Lambda}{K\Gamma}; t = MT; x = X\sqrt{\frac{M}{D_B}}.$$

Then the model (2.5) becomes:

$$\begin{cases} \partial_t b = \lambda w b(1-b)(1+\eta b)^2 - b + \nabla^2 b, \\ \partial_t w = p - \nu w(1-\rho b) - \lambda w b(1+\eta b)^2 + \delta_w \nabla^2 w, \end{cases} \tag{2.6}$$

where

$$\lambda = \frac{K\Gamma}{M}; \eta = EK; p = \frac{\Lambda P}{K\Gamma M}; \nu = \frac{N}{M}; \rho = R; \delta_w = \frac{D_W}{D_B}.$$

In the above model, all parameters are positive and have biological significance, and the parameter η and soil–water diffusivity δ_w determine the strength of the uptake–diffusion feedback. Next, we analyze the stability of equilibrium points of the model (2.6) and the conditions of producing Turing pattern.

2.2 Mathematical analysis of the model

2.2.1 Equilibrium points

When there is no diffusion term, our model (2.6) becomes:

$$\begin{cases} d_t b = \lambda w b(1-b)(1+\eta b)^2 - b, \\ d_t w = p - \nu w(1-\rho b) - \lambda w b(1+\eta b)^2. \end{cases} \tag{2.7}$$

The equilibrium point can be calculated by making the right end of Eq. (2.7) equal to zero (i.e. $\frac{\partial b}{\partial t} = 0$, $\frac{\partial w}{\partial t} = 0$). The model has two types of equilibria: (I) desert state $E_0(0, \frac{p}{\nu})$; (II) vegetation steady state $E^*(b^*, w^*)$.

Table 1 Description of the parameters in the model (2.5)

Parameter	Units	Description
Λ	$(\mathrm{kg/m^2})^{-1}\,\mathrm{year}^{-1}$	Conversion coefficient of plant water absorption into biomass
K	$\mathrm{kg/m^2}$	Maximum standing biomass
E	$(\mathrm{kg/m^2})^{-1}$	The root-to-shoot ratio
M	year^{-1}	Mortality rate
P	$\mathrm{kg/m^2\,year}^{-1}$	Precipitation rate
N	year^{-1}	Soil–water evaporation rate
R	–	Evaporation decreases due to shading (dimensionless)
Γ	$(\mathrm{kg/m^2})^{-1}\,\mathrm{year}^{-1}$	Soil–water consumption rate
D_B	$\mathrm{m^2/year}^{-1}$	Diffusion coefficient of seed
D_W	$\mathrm{m^2/year}^{-1}$	Diffusion coefficient of soil–water

For vegetation steady state $E^*(b^*, w^*)$, where $w^* = \frac{1}{\lambda(1+\eta b)^2(1-b)}$, and b^* satisfies the following equation:

$$\lambda\eta^2(p+1)b^3 + \lambda\eta(2p+2-\eta p)b^2 + (\lambda p + \lambda - 2\lambda\eta p - \nu\rho)b + \nu - \lambda p = 0 \tag{2.8}$$

and $0 < b < 1$ (to ensure that the equilibrium point has biological significance).

Denote

$$\begin{aligned} &c_1 = \lambda\eta^2(p+1), \quad c_2 = \lambda\eta(2p+2-\eta p), \quad c_3 = \lambda p + \lambda - 2\lambda\eta p - \nu\rho, \quad c_4 = \nu - \lambda p, \\ &A = c_2^2 - 3c_1c_3 = \lambda^2\eta^2(p+1+\eta p)^2 + 3\nu\rho\lambda\eta^2(p+1) > 0, \\ &B = c_2c_3 - 9c_1c_4 = \lambda\eta(2p+2-\eta p)(\lambda p + \lambda - 2\lambda\eta p - \nu\rho) - 9\lambda\eta^2(p+1)(\nu - \lambda p). \end{aligned}$$

Marking the left end of Eq. (2.8) as $f(b)$, and considering $f(0) = \nu - \lambda p2$, $f(1) = \lambda\eta^2 + 2\lambda\eta + \lambda - \nu\rho + \nu = 0$, we have $p = \frac{\nu}{\lambda}$, $\rho = 1 + \frac{\lambda(1+\eta)^2}{\nu}$, which divides the two-dimensional plane into four regions (see Fig. 2). Next, we study the equilibrium points of each region:

(i) $f(0) > 0$, $f(1) > 0$.
Case 1. Equations (2.8) only one positive roots if $f(b_{\min}) = 0$, and (see Fig. 3(a1))

$$b^* = b_{\min} = \frac{\lambda(\eta p - 2p - 2) + \sqrt{\lambda^2(\eta p + p + 1)^2 + 3\lambda\nu\rho(p+1)}}{3\lambda\eta(p+1)}.$$

Case 2. Equation (2.8) has two positive roots if $f(b_{\min}) < 0$, and (see Fig. 3(a2))

$$b_1^* = \frac{\lambda(\eta p - 2p - 2) + 2\sqrt{\lambda^2(\eta p + p + 1)^2 + 3\lambda\nu\rho(p+1)}cos\left(\frac{\theta+\pi}{3}\right)}{3\lambda\eta(p+1)},$$

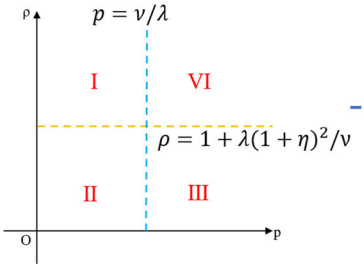

Region	condition	Number of equilibrium points
I	$f(0) > 0$ $f(1) < 0$	only one equilibrium point
II	$f(0) > 0$ $f(1) > 0$	two equilibrium point
III	$f(0) < 0$ $f(1) > 0$	only one equilibrium point
VI	$f(0) < 0$ $f(1) < 0$	no equilibrium point

Fig. 2 Distribution of equilibrium points. The figure on the left shows the four areas where the equilibrium points are distributed, and the table on the right shows the details of each area

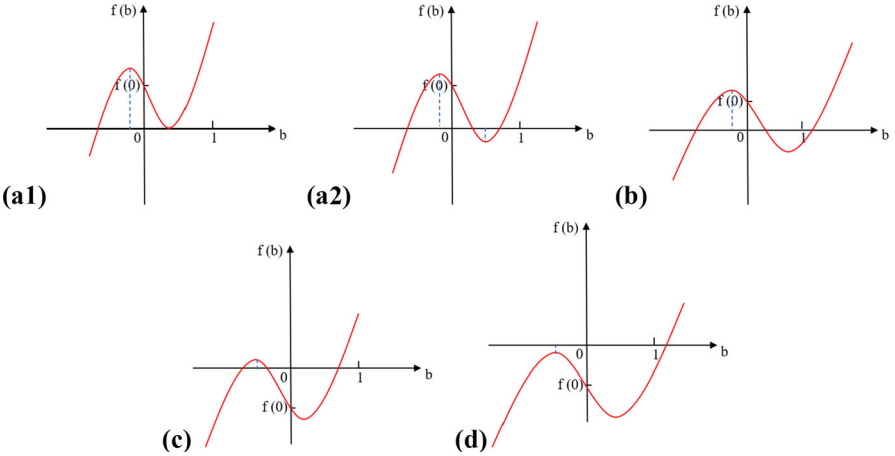

Fig. 3 Graph of the unary cubic function $f(b)$. **a1**, **a2** $f(0) > 0$, $f(1) > 0$; **b** $f(0) > 0$, $f(1) < 0$; **c** $f(0) < 0$, $f(1) > 0$; **d** $f(0) < 0$, $f(1) < 0$

$$b_2^* = \frac{\lambda(\eta p - 2p - 2) + 2\sqrt{\lambda^2(\eta p + p + 1)^2 + 3\lambda\nu\rho(p+1)}cos\left(\frac{\theta-\pi}{3}\right)}{3\lambda\eta(p+1)},$$

where $\theta = \arccos(T)$, $T = \dfrac{2Ac_2 - 3c_1B}{2\sqrt{A^3}}$.

(ii) $f(0) > 0$, $f(1) < 0$, Eq. (2.8) only one positive root b_1^* (see Fig. 3b).
(iii) $f(0) < 0$, $f(1) > 0$, Eq. (2.8) only one positive root b_2^* (see Fig. 3c).
(iv) $f(0) < 0$, $f(1) < 0$, Eq. (2.8) has no positive root (see Fig. 3d).

In summary, there are three forms of expression of the non-trivial equilibrium points: $E^*(b^*, w^*)$, $E_1^*(b_1^*, w_1^*)$ and $E_2^*(b_2^*, w_2^*)$. For $E^*(b^*, w^*)$, it's very difficult for us to calculate the existence condition $f(b_{\min}) = 0$, Therefore we only list this possible case here and will not discuss it further. For $E_1^*(b_1^*, w_1^*)$, it is always unstable, so in the following discussion, we will only analyze the equilibrium point $E_2^*(b_2^*, w_2^*)$.

2.2.2 Linear stability analysis

For model (2.7), the Jacobian matrix at the equilibrium point E_2^* is

$$J = \begin{pmatrix} \dfrac{b_2^*(3\eta b_2^* - 2\eta + 1)}{(1+\eta b_2^*)(b_2^* - 1)} & \lambda b_2^*(1 - b_2^*)(1+\eta b_2^*)^2 \\ \dfrac{3\lambda\eta^2 b^2 + 4\lambda\eta b_2^* + \lambda - \nu\rho}{\lambda(1+\eta b_2^*)^2(b_2^* - 1)} & \nu(\rho b_2^* - 1) - \lambda b_2^*(1+\eta b_2^*)^2 \end{pmatrix} = \begin{pmatrix} a_{11} & a_{12} \\ a_{21} & a_{22} \end{pmatrix}. \tag{2.9}$$

Thus, the eigenvalues $\lambda \in \mathbb{C}$ satisfy

$$\lambda^2 - tr(J)\lambda + \Delta(J) = 0, \tag{2.10}$$

where

$$\begin{aligned} tr(J) &= a_{11} + a_{22} = \frac{b_2^*(3\eta b_2^* - 2\eta + 1)}{(1+\eta b_2^*)(b_2^* - 1)} + \nu(\rho b_2^* - 1) - \lambda b_2^*(1+\eta b_2^*)^2, \\ \Delta(J) &= a_{11}a_{22} - a_{12}a_{21}, \\ &= \frac{(b_2^{*3}\eta^3\lambda + 3b_2^{*2}\eta^2\lambda - 2b_2^{*2}\eta\nu\rho + b_2^*\eta\nu\rho + 3b_2^*\eta\lambda + 3b_2^*\eta\nu - 2\eta\nu - \nu\rho + \lambda + \nu)b_2^*}{(b_2^*\eta + 1)(1 - b_2^*)}. \end{aligned}$$

All eigenvalues $\lambda \in \mathbb{C}$ have negative real parts (i.e. $\Re(\lambda) < 0$) if $2\eta < 3\eta b_2^* + 1$ and $\nu\rho < 3\lambda\eta^2 b_2^{*2} + 4\lambda\eta b_2^* + \lambda$. Then E_2^* is locally stable in the absence of diffusion.

If diffusion term is considered, then the Jacobian matrix for the equilibrium point $E_2^*(b_2^*, w_2^*)$ is given by

$$J = \begin{pmatrix} a_{11} - k^2 & a_{12} \\ a_{21} & a_{22} - k^2\delta_w \end{pmatrix}. \tag{2.11}$$

Thus, the characteristic equation can be obtained as follows:

$$\lambda_k^2 - tr_k(J)\lambda + \Delta_k(J) = 0, \tag{2.12}$$

where

$$\begin{aligned} tr_k(J) &= a_{11} + a_{22} - k^2(1 + \delta_w), \\ \Delta_k(J) &= a_{11}a_{22} - a_{12}a_{21} - k^2(\delta_w a_{11} + a_{22}) + k^4\delta_w. \end{aligned}$$

Turing bifurcation will occur if

$$\delta_w a_{11} + a_{22} > 2\sqrt{\delta_w det(J)}.$$

Next, we select ρ as the control variable. Due to the algebraic complexity of the equilibrium point and the eigenvalue, we cannot directly display the critical value of

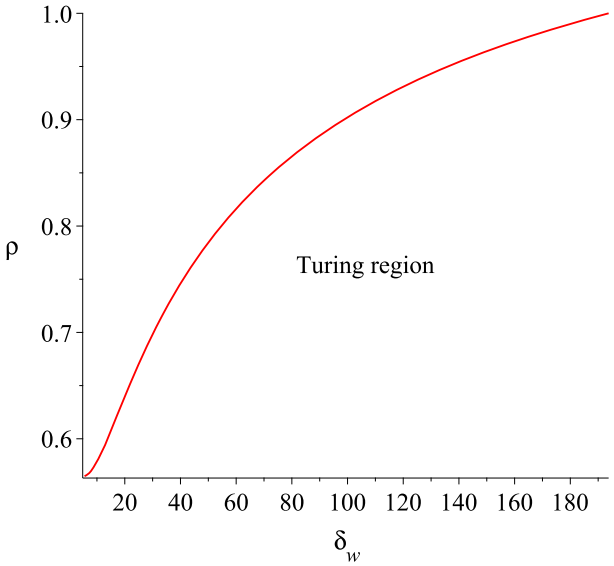

Fig. 4 Bifurcation diagram of system (2.6). It shows the Turing area that can produce patterns on the $\rho O \delta_w$ plane. The parameter values are $p = 1.5179$, $\eta = 2.8$, $\lambda = 0.4571$, $\nu = 1.4286$

the Hopf branch and Turing branch. Therefore, we use numerical methods to solve the Turing region (see Fig. 4). We can find that under this set of parameter values, the equilibrium point remains stable under uniform disturbances in space. Consequently, we only need to ensure that the equilibrium point is unstable under non-uniform spatial disturbances. At the same time, we can get the dispersion diagram of model (2.6) (see Fig. 5). Obviously, Fig. 5 shows that within an appropriate parameter range, as the parameter ρ decreases, the real part of the eigenvalue gradually increases, and the Turing patterns appear.

3 Amplitude equations

The amplitude equation is a kind of equation which can describe the dynamical behavior of the system near the most unstable mode. Therefore, the amplitude equation is a good tool when we want to study the dynamic behavior of the system near the Turing bifurcation point (i.e. the most unstable mode) (Sun et al. 2018; Ouyang 2000; Lejeune et al. 2004; Zhang et al. 2012; Sun 2016). The pattern of the system can be described by three pairs of wave vectors k_1, k_2, k_3, and they are 120° angle with each other. The expression of amplitude equation is as follows:

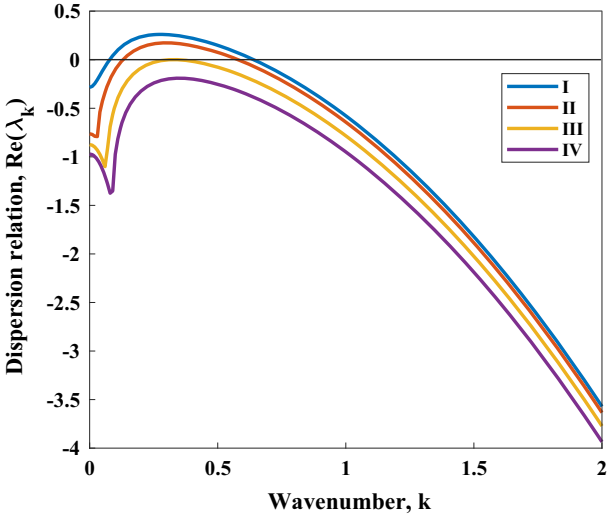

Fig. 5 Dispersion diagram visualization of dispersion relation for different values of parameter ρ. (I) $\rho = 0.6$, (II) $\rho = 0.7$, (III) $\rho = 0.9372$, (IV) $\rho = 1.2$. The other parameter values are $\eta = 2.8$, $\lambda = 0.4571$, $\nu = 1.4286$, $p = 1.5179$, $\delta_w = 125$

$$\begin{cases} \tau_0 \dfrac{\partial A_1}{\partial t} = \mu A_1 + h\bar{A}_2\bar{A}_3 - [g_1|A_1|^2 + g_2(|A_2|^2 + |A_3|^2)]A_1, \\ \tau_0 \dfrac{\partial A_2}{\partial t} = \mu A_2 + h\bar{A}_1\bar{A}_3 - [g_1|A_1|^2 + g_2(|A_2|^2 + |A_3|^2)]A_2, \\ \tau_0 \dfrac{\partial A_3}{\partial t} = \mu A_3 + h\bar{A}_1\bar{A}_2 - [g_1|A_1|^2 + g_2(|A_2|^2 + |A_3|^2)]A_3. \end{cases} \tag{3.1}$$

Next, the most important thing is to calculate the coefficients of the amplitude equation, which we can do through multi-scale analysis. Here, we choose ρ as the control parameter.

Firstly, rewrite the model (2.6) at the equilibrium point $E_2^*(b_2^*, w_2^*)$ as follows:

$$\begin{cases} \partial_t x = a_{11}x + a_{12}y + N_1(x, y) + \nabla^2 x, \\ \partial_t y = a_{21}x + a_{22}y + N_2(x, y) + \delta_w \nabla^2 y, \end{cases} \tag{3.2}$$

where x, y are simple substitutions for b and w in system (2.6).

The solution of system (3.2) at the critical point $\rho = \rho_T$ can be expressed as:

$$c = \begin{pmatrix} x \\ y \end{pmatrix} = \sum_{i=1}^{3} \begin{pmatrix} A_i^x \\ A_i^y \end{pmatrix} e^{ik_i r} + c.c., \tag{3.3}$$

Table 2 The expansion of ρ, N, L and c

The expanded quantity	The expand mode
ρ	$\rho_T - \rho = \varepsilon\rho_1 + \varepsilon^2\rho_2 + \cdots$
N	$N = \varepsilon^2 h^2 + \varepsilon^3 h^3 + o(\varepsilon^4)$
L	$L = L_T + (\rho_T - \rho)M$
c	$c = \begin{pmatrix} x \\ y \end{pmatrix} = \varepsilon \begin{pmatrix} x_1 \\ y_1 \end{pmatrix} + \varepsilon^2 \begin{pmatrix} x_2 \\ y_2 \end{pmatrix} + \cdots .$

ε is a small parameter

then the system (3.2) can be written as:

$$\frac{\partial c}{\partial t} = Lc + N(c, c), \tag{3.4}$$

where L is a linear operator and N is a nonlinear operator, and

$$L = \begin{pmatrix} a_{11} + \Delta & a_{12} \\ a_{21} & a_{22} + \delta_w \Delta \end{pmatrix}, N = \begin{pmatrix} N_1(x, y) \\ N_2(x, y) \end{pmatrix}.$$

For our system, we only study the dynamical behavior of the system near the critical point ρ_T. Therefore, we expand the control parameters ρ, linear operators L, nonlinear operators N, and variable c. For the specific expansion form, see Table 2, and

$$L_T = \begin{pmatrix} a_{11}^* + \Delta & a_{12}^* \\ a_{21}^* & a_{22}^* + \delta_w \Delta \end{pmatrix}, M = \begin{pmatrix} b_{11} & b_{12} \\ b_{21} & b_{22} \end{pmatrix}.$$

The core of multi-scale analysis method is to study the dynamic behavior of the system according to different time or space scales. Here, we separate the time scales of the system (3.4), let

$$\frac{\partial}{\partial t} = \frac{\partial}{\partial T_0} + \varepsilon \frac{\partial}{\partial T_1} + \varepsilon^2 \frac{\partial}{\partial T_2} + \cdots . \tag{3.5}$$

Since the amplitude A is a slow variable, and the time derivative $\frac{\partial}{\partial T_0}$ is a fast variable, so $\frac{\partial}{\partial T_0}$ has no effect on the amplitude A, so we can get:

$$\frac{\partial A}{\partial t} = \varepsilon \frac{\partial A}{\partial T_1} + \varepsilon^2 \frac{\partial A}{\partial T_2} + \cdots . \tag{3.6}$$

Substituting the expansion formula in Table 2 and (3.6) into (3.4), we can get the equations of different order of ε (see Table 3).

For the order of ε

$$L_T \begin{pmatrix} x_1 \\ y_1 \end{pmatrix} = 0, \tag{3.7}$$

Table 3 The corresponding equations of different orders of ε

The order	The corresponding equation
ε	$L_T \begin{pmatrix} x_1 \\ y_1 \end{pmatrix} = 0$
ε^2	$L_T \begin{pmatrix} x_2 \\ y_2 \end{pmatrix} = \frac{\partial}{\partial T_1} \begin{pmatrix} x_1 \\ y_1 \end{pmatrix} - \rho_1 M \begin{pmatrix} x_1 \\ y_1 \end{pmatrix} - h^2$
ε^3	$L_T \begin{pmatrix} x_3 \\ y_3 \end{pmatrix} = \frac{\partial}{\partial T_1} \begin{pmatrix} x_2 \\ y_2 \end{pmatrix} + \frac{\partial}{\partial T_2} \begin{pmatrix} x_1 \\ y_1 \end{pmatrix} - \rho_1 M \begin{pmatrix} x_2 \\ y_2 \end{pmatrix} - \rho_2 M \begin{pmatrix} x_1 \\ y_1 \end{pmatrix} - h^3$

where L_T is the linear operator of the system at the critical point, and $\begin{pmatrix} x_1 \\ y_1 \end{pmatrix}$ is a linear combination of the eigenvectors corresponding to the zero eigenvalues of the linear operator L_T. By solving the above equations, we can gain:

$$\begin{pmatrix} x_1 \\ y_1 \end{pmatrix} = l(W_1 e^{ik_1 r} + W_2 e^{ik_2 r} + W_3 e^{ik_3 r}) + c.c., \tag{3.8}$$

where $l = \begin{pmatrix} \dfrac{\delta_w a_{11}^* - a_{22}^*}{2a_{21}^*} \\ 1 \end{pmatrix}$, and $|k_i| = k_T$ (i=1,2,3), c.c. represents the conjugate of the right term, and W_i is the amplitude corresponding to the mode $e^{ik_i r}$ of the system under the first-order perturbation, and its form is determined by the higher-order perturbation term.

For the order of ε^2

$$L_T \begin{pmatrix} x_2 \\ y_2 \end{pmatrix} = \frac{\partial}{\partial T_1} \begin{pmatrix} x_1 \\ y_1 \end{pmatrix} - \rho_1 M \begin{pmatrix} x_1 \\ y_1 \end{pmatrix} - h^2 = \begin{pmatrix} F_x \\ F_y \end{pmatrix}. \tag{3.9}$$

According to the Fredholm solvability condition, in order to ensure the existence of non-trivial solutions of Eq. (3.9), the vector function at the right end of Eq. (3.9) must be orthogonal to the zero eigenvector of operator L_T^+. Where L_T^+ represents the conjugate operator of L_T, i.e

$$L_T^+ = \begin{pmatrix} a_{11}^* - k_T^2 & a_{21}^* \\ a_{12}^* & a_{22}^* - \delta_w k_T^2 \end{pmatrix}.$$

Then, the zero eigenvector of L_T^+ is

$$\begin{pmatrix} 1 \\ -\dfrac{\delta_w a_{11}^* - a_{22}^*}{2\delta_w a_{21}^*} \end{pmatrix} e^{-ik_i r} + c.c. \tag{3.10}$$

Let F_x^i and F_y^i denote the coefficients corresponding to $e^{ik_i r}$ in F_x and F_y respectively, so we can get the following equation:

$$\begin{pmatrix} F_x^1 \\ F_y^1 \end{pmatrix} = \begin{pmatrix} l\dfrac{\partial W_1}{\partial T_1} \\ \dfrac{\partial W_1}{\partial T_1} \end{pmatrix} - \rho_1 \begin{pmatrix} lb_{11} + b_{12} \\ lb_{21} + b_{22} \end{pmatrix} W_1 - \begin{pmatrix} h_1 \\ h_2 \end{pmatrix} \bar{W}_2 \bar{W}_3, \tag{3.11}$$

We can get the remaining two equations by changing the subscript.

According to the conjugate condition $\left(1 - \dfrac{l}{\delta_w}\right)\begin{pmatrix} F_x^i \\ F_y^i \end{pmatrix} = 0$ (i=1,2,3), we have:

$$\begin{cases} \dfrac{(\delta_w - 1)l}{\delta_w}\dfrac{\partial W_1}{\partial T_1} = E_1 W_1 + \left(h_1 - \dfrac{l}{\delta_w} h_2\right) \bar{W}_2 \bar{W}_3, \\ \dfrac{(\delta_w - 1)l}{\delta_w}\dfrac{\partial W_2}{\partial T_1} = E_1 W_2 + \left(h_1 - \dfrac{l}{\delta_w} h_2\right) \bar{W}_1 \bar{W}_3, \\ \dfrac{(\delta_w - 1)l}{\delta_w}\dfrac{\partial W_3}{\partial T_1} = E_1 W_3 + \left(h_1 - \dfrac{l}{\delta_w} h_2\right) \bar{W}_1 \bar{W}_2. \end{cases} \tag{3.12}$$

The above Eq. (3.12) is an amplitude equations under with first-order perturbation. We can find that the coefficient of the second order term of the amplitude equation is greater than zero, so the amplitude $W_i (i = 1, 2, 3)$ diverges. In this case, we need to introduce higher-order terms to make it saturated. Therefore, the solution of Eq. (3.9) is written as follows:

$$\begin{aligned} \begin{pmatrix} x_2 \\ y_2 \end{pmatrix} = \begin{pmatrix} X_0 \\ Y_0 \end{pmatrix} + \sum_{i=1}^{3} \begin{pmatrix} X_i \\ Y_i \end{pmatrix} e^{ik_i r} + \sum_{i=1}^{3} \begin{pmatrix} X_{ii} \\ Y_{ii} \end{pmatrix} e^{2ik_i r} + \begin{pmatrix} X_{12} \\ Y_{12} \end{pmatrix} e^{i(k_1 - k_2)r} \\ + \begin{pmatrix} X_{23} \\ Y_{23} \end{pmatrix} e^{i(k_2 - k_3)r} + \begin{pmatrix} X_{31} \\ Y_{31} \end{pmatrix} e^{i(k_3 - k_1)r} + c.c., \end{aligned} \tag{3.13}$$

where,

$$\begin{pmatrix} X_0 \\ Y_0 \end{pmatrix} = \begin{pmatrix} x_0 \\ y_0 \end{pmatrix} (|W_1|^2 + |W_2|^2 + |W_2|^2), \qquad X_i = lY_i,$$
$$\begin{pmatrix} X_{ii} \\ Y_{ii} \end{pmatrix} = \begin{pmatrix} x_{11} \\ y_{11} \end{pmatrix} W_j^2, \qquad \begin{pmatrix} X_{ik} \\ Y_{ik} \end{pmatrix} = \begin{pmatrix} x_* \\ y_* \end{pmatrix} W_i \bar{W}_k,$$

For the order of ε^3

$$L_T \begin{pmatrix} x_3 \\ y_3 \end{pmatrix} = \frac{\partial}{\partial T_1}\begin{pmatrix} x_2 \\ y_2 \end{pmatrix} + \frac{\partial}{\partial T_2}\begin{pmatrix} x_1 \\ y_1 \end{pmatrix} - \rho_1 M \begin{pmatrix} x_2 \\ y_2 \end{pmatrix} - \rho_2 M \begin{pmatrix} x_1 \\ y_1 \end{pmatrix} - h^3 = \begin{pmatrix} H_x \\ H_y \end{pmatrix}. \tag{3.14}$$

The method is similar to the calculation process of Eq. (3.9), and we can obtain:

$$\begin{aligned}\frac{(\delta_w-1)l}{\delta_w}\left(\frac{\partial Y_1}{\partial T_1}+\frac{\partial W_1}{\partial T_2}\right)&=(\rho_1 Y_1+\rho_2 W_1)\left[lb_{11}+b_{12}-\frac{l}{\delta_w}(lb_{21}+b_{22})\right]W_1\\&-\left[\left(M_{11}-\frac{l}{\delta_w}M_{21}\right)|W_1|^2\right.\\&\left.+\left(M_{12}-\frac{l}{\delta_w}M_{22}\right)(|W_2|^2+|W_2|^2)\right]W_1\\&+\left(h_1-\frac{l}{\delta_w}h_2\right)(\bar{W}_2\bar{Y}_3+\bar{W}_3\bar{Y}_2).\end{aligned}\tag{3.15}$$

Similarly, the other two equations can be obtained by changing the subscript.

The amplitude A_i can be expanded as:

$$A_i=\varepsilon W_i+\varepsilon^2 Y_i+o(\varepsilon^3).\tag{3.16}$$

Combining Eqs. (3.12), (3.15) and (3.16), we can obtain the amplitude equation as follows:

$$\tau_0\frac{\partial A_1}{\partial t}=\mu A_1+h\bar{A}_2\bar{A}_3-[g_1|A_1|^2+g_2(|A_2|^2+|A_3|^2)]A_1,\tag{3.17}$$

where the specific expression of each coefficient is shown in Table 4. Expressions for parameters not given in this section are in the "Appendix A".

Each amplitude can be decomposed into the product of its mode $\kappa_i=|A_i|$ and the corresponding phase angle φ_i, i.e. $A_i=\kappa_i e^{i\varphi_i}$. Substituting it into the amplitude equation (3.1) above and separating the real part and the imaginary part, we can get the following system:

$$\begin{cases}\tau_0\dfrac{\partial\varphi}{\partial t}=-h\dfrac{\kappa_1^2\kappa_2^2+\kappa_1^2\kappa_3^2+\kappa_2^2\kappa_3^2}{\kappa_1\kappa_2\kappa_3}sin\varphi,\\ \tau_0\dfrac{\partial\varphi}{\partial t}=\mu\kappa_1+h\kappa_2\kappa_3 cos\varphi-g_1\kappa_1^3-g_2(\kappa_2^2+\kappa_3^2)\kappa_1,\\ \tau_0\dfrac{\partial\varphi}{\partial t}=\mu\kappa_2+h\kappa_1\kappa_3 cos\varphi-g_1\kappa_2^3-g_2(\kappa_1^2+\kappa_3^2)\kappa_2,\\ \tau_0\dfrac{\partial\varphi}{\partial t}=\mu\kappa_3+h\kappa_1\kappa_2 cos\varphi-g_1\kappa_3^3-g_2(\kappa_1^2+\kappa_2^2)\kappa_3,\end{cases}\tag{3.18}$$

where $\varphi=\varphi_1+\varphi_2+\varphi_3$. This system (3.1) has four different types of solutions, corresponding to four different pattern structures, see Table 5 for details.

Table 4 The corresponding expression of each coefficient in Eq. (3.17)

The coefficient	The corresponding expression
τ_0	$\dfrac{l(\delta_w-1)}{\delta_w\rho_T\left[lb_{11}+b_{12}-\dfrac{l}{\delta_w}(lb_{21}+b_{22})\right]}$
μ	$\dfrac{\rho_T-\rho}{\rho_T}$
h	$\dfrac{-2m_{12}w_2^*l^2+\dfrac{2(a_{11}+1)l}{w_2^*}+\dfrac{l}{\delta_w}\left(2m_{21}w_2^*l^2-\dfrac{2a_{21}l}{w_2^*}\right)}{\rho_T\left[lb_{11}+b_{12}-\dfrac{l}{\delta_w}(lb_{21}+b_{22})\right]}$
g_1	$\dfrac{\left(M_{11}-\dfrac{l}{\delta_w}M_{21}\right)}{\rho_T\left[lb_{11}+b_{12}-\dfrac{l}{\delta_w}(lb_{21}+b_{22})\right]}$
g_2	$\dfrac{\left(M_{12}-\dfrac{l}{\delta_w}M_{22}\right)}{\rho_T\left[lb_{11}+b_{12}-\dfrac{l}{\delta_w}(lb_{21}+b_{22})\right]}$

4 Main results

4.1 Pattern structures of vegetation

For the spatial model, we can not use the analysis method to study its spatial dynamics. Therefore, in this section, we use the computer to carry out the numerical simulation. We choose a region of size 200×200 whose boundary satisfies Neumann boundary conditions. We set the time region as [0,10,000], the time step as $\Delta t = 0.1$, and the space step as $\Delta h = 2$. The initial value is the random perturbation at the equilibrium point E_2^*.

We use numerical simulation to verify the above theoretical analysis. Selecting the values of different parameters λ, η, ν, δ and p, we can calculate the values of h, g_1, g_2, μ_1, μ_2, μ_3 and μ_4 according to the expression of the amplitude equation coefficients in Sect. 3. In order to observe the pattern structure of vegetation, we selected three sets of parameter values in Table 5, and the corresponding results are shown in Fig. 6. We can find that when the first set of parameter values are taken, μ is between μ_2 and μ_3, and the system (2.6) presents a spot pattern (see Fig. 6a); when the second set of parameter values is taken, μ is between Between μ_3 and μ_4, the spot pattern loses its stability, and the strip pattern begins to appear, showing a mixed pattern (see Fig. 6b); when the third set of parameter values is taken, μ is greater than μ_4, and the spot pattern disappears. It becomes a striped pattern (see Fig. 6c).

Table 5 Analysis of the existence and stability of the pattern of Eq. (3.18)

Pattern type	Expression	Existence range	Stability
Homogeneous state	$\kappa_1 = \kappa_2 = \kappa_3 = 0$	Arbitrary range	$\mu < \mu_2$ stable $\mu > \mu_2$ unstable
Dot pattern	$\kappa_+ = \frac{\lvert h\rvert + \sqrt{h^2 + 4\mu(g_1 + 2g_2)}}{2(g_1 + 2g_2)} \kappa_- = \frac{\lvert h\rvert - \sqrt{h^2 + 4\mu(g_1 + 2g_2)}}{2(g_1 + 2g_2)}$	$H_0 : h > 0\, H_\pi : h < 0\, \mu > \mu_1$	$\kappa_+ : \mu < \mu_4$ stable κ_- : unstable
Strip pattern	$\kappa_1 = \sqrt{\frac{\mu}{g_1}} \neq 0\, \kappa_2 = \kappa_3 = 0$	$\mu > 0$	$\mu > \mu_3$ stable $\mu < \mu_3$ unstable
Mixed pattern	$\kappa_1 = \frac{\lvert h\rvert}{g_2 - g_1} \kappa_2 = \kappa_3 = \sqrt{\frac{\mu - g_1\kappa_1^2}{g_1 + g_2}}$	$\mu > \mu_3$	Unstable

$\mu_1 = \frac{-h^2}{4(g_1 + 2g_2)}, \mu_2 = 0, \mu_3 = \frac{h^2 g_1}{(g_2 - g_1)^2}, \mu_4 = \frac{2g_1 + g_2}{(g_2 - g_1)^2} h^2.$

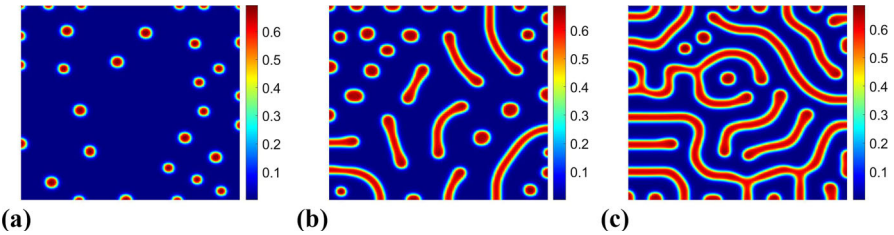

Fig. 6 The pattern structure corresponding to different values of parameter ρ.The values of each parameter are shown in Table 6

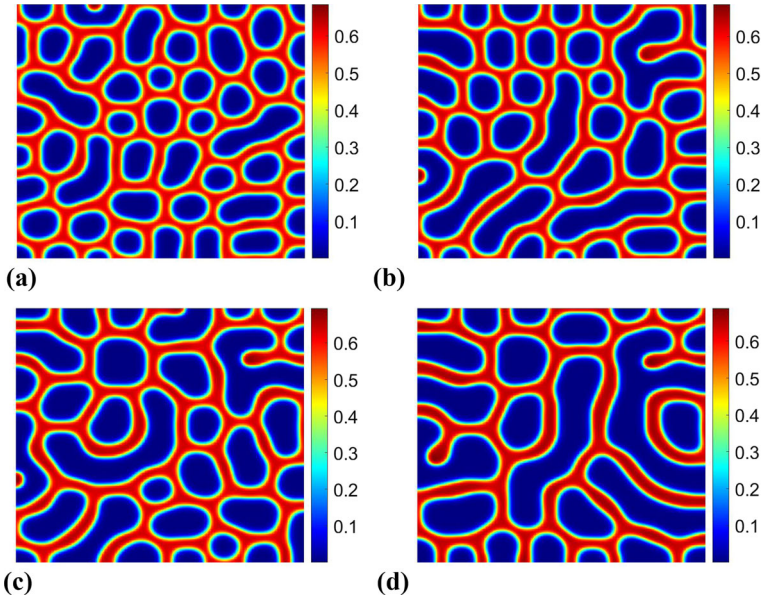

Fig. 7 The pattern structure corresponding to different values of parameter δ_w. **a** $\delta_w = 125$; **b** $\delta_w = 160$; **c** $\delta_w = 200$; **d** $\delta_w = 250$. The other parameter values are $\eta = 2.8$, $\lambda = 0.4571$, $\nu = 1.4286$, $p = 1.6247$, $\rho = 0.7$

4.2 Influence of water diffusion and shading on vegetation patterns

Next, we study the influence of some parameters on vegetation patterns. In our model, only a single feedback of soil–water diffusion is captured. The feedback of soil–water diffusion is not only related to the soil–water diffusion coefficient, but also to the root and shoot characteristics of vegetation. It is reflected in the parameters δ_w and η in our dimensionless model. Therefore, we studied the influence of parameters δ_w and η on vegetation patterns. Figure 7 shows the change of the corresponding vegetation pattern with the change of parameter δ_w. We can find that with the gradual increase of parameter δ_w, the gap size is also increasing, while the average biomass of vegetation is gradually decreasing (see Fig. 8). This is negatively related to parameter δ_w.

Table 6 The values of each parameter in Fig. 4

Older	λ	ν	η	p	ρ	δ_w	h	μ	Range of μ
1	0.4571	1.4286	2.8	1.4065	1	125	11.38582686	0.161360121	(μ_2, μ_3)
2	0.4571	1.4286	2.8	1.5179	0.7	125	10.86821033	0.3389224000	(μ_3, μ_4)
3	0.4571	1.4286	2.8	1.7024	0.2648	125	15.76564631	1.126027504	(μ_4, ∞)

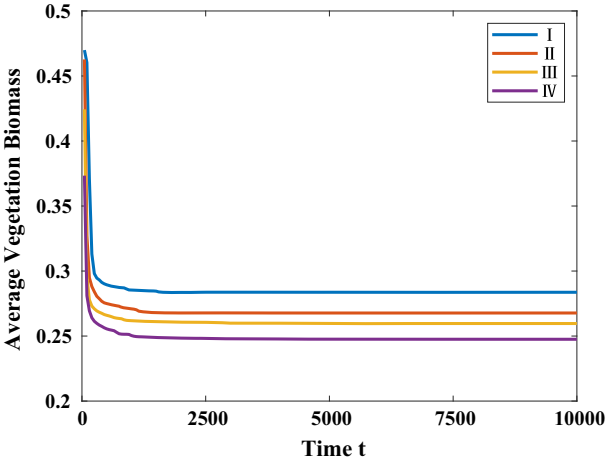

Fig. 8 When the parameter δ_w takes different values, the average biomass of vegetation changes with time t. (I) $\delta_w = 125$, (II) $\delta_w = 160$, (III) $\delta_w = 200$, (IV) $\delta_w = 250$. The values of other parameters see Fig. 7

In Fig. 9, we consider the effect of parameter η on the vegetation pattern. When the parameter η is small, the spot pattern appears (Fig. 9a); when the parameter η increases slightly, the spot pattern begins to disappear, the strip pattern appears, showing the spot strip mixed pattern (Fig. 9b); as the parameter η continues to increase, the spot pattern completely disappears, and the strip pattern appears (Fig. 9c, d); when the parameter η further increases, the gap pattern appears (Fig. 9e, f). To sum up, with the increase of parameter η, the vegetation pattern changes in the following sequence: spot pattern, mixed pattern, labyrinth pattern and gap pattern. Figure 10 shows the relationship between parameter η and the average biomass of vegetation. Obviously, with the increase of parameter η, the average biomass of vegetation increased, which was positively correlated.

Shading affects the growth of vegetation and regulates the metabolism of vegetation (Gommers et al. 2013). The effect of shading is also considered in system 2.6, which refers to the reduction of water evaporation due to shading. That is to say, the available water of vegetation increases. We use numerical simulation to study the effect of shading parameters on vegetation pattern structure. The results show that the enhancement of shading effect is beneficial to the growth of vegetation, and with the increase of shading parameters, spot pattern, strip pattern and gap pattern appear in turn (Fig. 11).

4.3 Gradual transitions from uniform state to gap pattern

Through numerical simulation, we show that there is a gradual transition in the bistable range of uniform vegetation and gap pattern state, as shown in Fig. 12. This localized state expands and merges until it reaches an almost periodic gap pattern, that is, a gradual regime shifts occurs (Bel et al. 2012; Zelnik et al. 2013, 2017), which is consistent with the conclusion of Zelnik et al. (2015). Ecosystem state transitions are considered to be abrupt global transitions from a stable state to an alternative

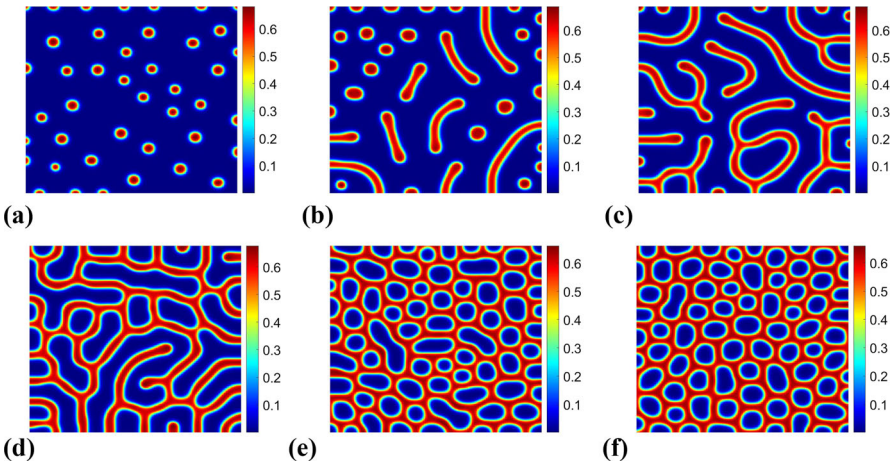

Fig. 9 The pattern structure corresponding to different values of parameter η. **a** $\eta = 2.65$; **b** $\eta = 2.8$; **c** $\eta = 2.9$; **d** $\eta = 3.1$; **e** $\eta = 3.3$; **f** $\eta = 3.4$. The other parameter values are $p = 1.5179$, $\lambda = 0.4571$, $\nu = 1.4286$, $\rho = 0.7$, $\delta_w = 125$

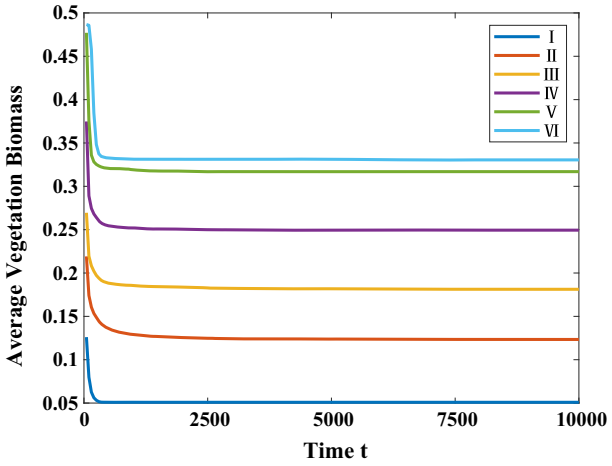

Fig. 10 When the parameter η takes different values, the average biomass of vegetation changes with time t. (I) $\eta = 2.65$, (II) $\eta = 2.8$, (III) $\eta = 2.9$, (IV) $\eta = 3.1$, (V) $\eta = 3.3$, (VI) $\eta = 3.4$. The values of other parameters see Fig. 9

stable state caused by small environmental changes. In general, this sudden response is unfavorable to the ecosystem, because it will lead to the loss of biological productivity and biodiversity, and then affect the function and stability of the ecosystem (Bel et al. 2012; Yachi and Loreau 1999; Loreau et al. 2001). However, in a spatially expanding ecosystem, the transition can also be gradual (see Fig. 12). A water-limited vegetation dynamic model shows that when the rainfall rate is high, the system may be in the bistable range of uniform vegetation and pattern state, and there is a localized state in this range. Therefore, the desertification process may be gradual, but with the decrease

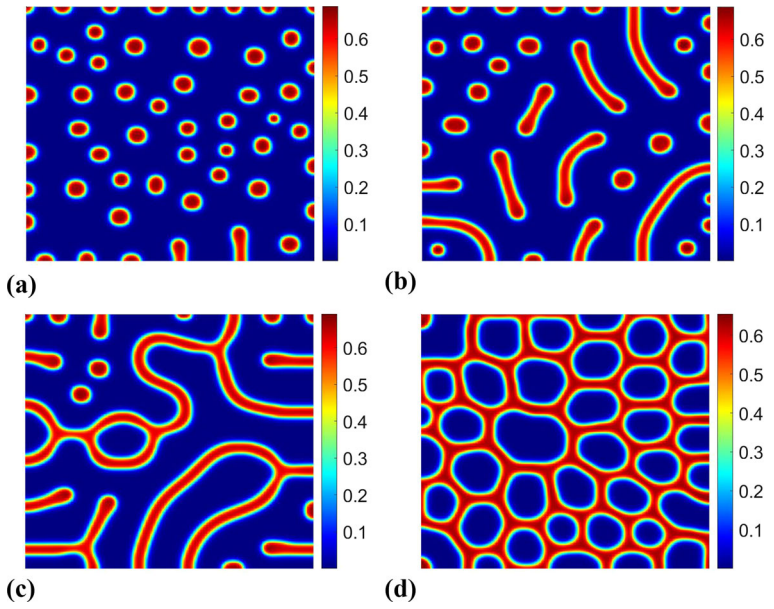

Fig. 11 Effects of shading parameters ρ on vegetation pattern structure. **a** $\rho = 0.6$; **b** $\rho = 0.7$; **c** $\rho = 0.8$; **d** $\rho = 0.94$. The other parameter values are $\eta = 2.8$, $\lambda = 0.4571$, $\nu = 1.4286$, $p = 1.5179$, $\delta_w = 125$

of rainfall rate, the system is close to the bare soil state, and the desertification process tends to be more abrupt. Because there is no localized state in the bistable range of bare soil state and pattern state (Zelnik et al. 2016).

4.4 Comparison between Gilad model (2.1) and simplified model (2.5)

This section mainly compares Gilad model with its simplified model from three aspects: pattern structure, the average vegetation biomass and the spatial distribution. For numerical simulation, the forward difference method is used to discretize the model. The initial condition is set as random disturbance near the equilibrium point, and the boundary condition is periodic boundary. Meanwhile, in order to make the comparison results of the two models more convincing, the same parameter value is selected in the numerical simulation (see Table 7).

Firstly, the pattern structure of Gilad model and its simplified model is compared in Fig. 13. For the Gilad model, vegetation rapidly evolves from the initial uniform state, gradually emerges a spot structure and ultimately forms a very periodic spot pattern. For the simplified model, the initial state of vegetation is uniform, and the spot patch progressively appears with the increase of time, and eventually these patches exhibit a certain regular distribution. Consequently, from the perspective of their structure, they are both spot patterns with comparatively consistent structures. Nonetheless, there are some subtle differences in their evolution process, that is, the evolution process of Gilad model is more periodic, and it takes less time to form the pattern structure.

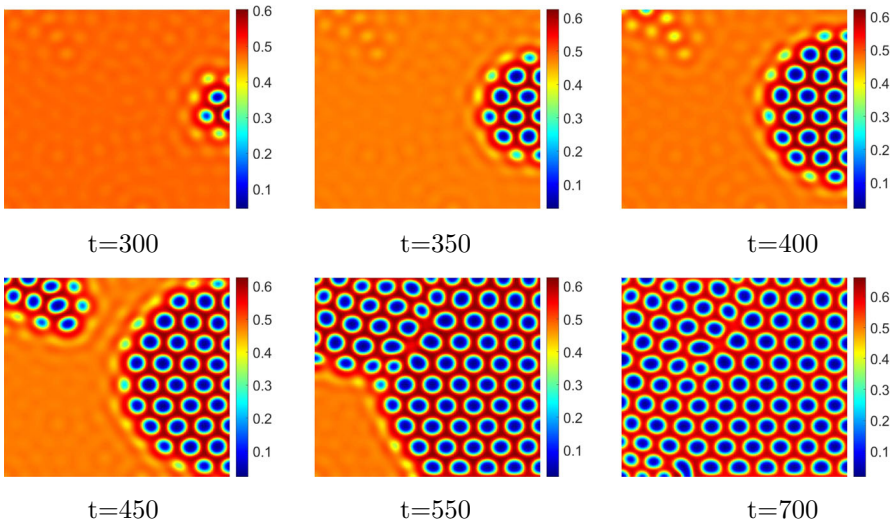

Fig. 12 A gradual regime shifts. The values of relevant parameters are $\eta = 4.5$, $\lambda = 1.357$, $\nu = 1.4286$, $p = 1.045$, $\rho = 0.7$, $\delta_w = 250$. The simulated domains are 150×150

Table 7 Values of relevant parameters in Gilad and simplified model

Parameter	Value	Parameter	Value	Parameter	Value
E	3.5	Λ	0.032	Q	0.05
K	1	R	0.95	f	0.1
M	1.2	P	146.25	D_B	6.25×10^{-4}
N	4	Γ	20	D_W	6.25×10^{-2}

Secondly, the average vegetation biomass of Gilad is compared with that of its simplified model. In Fig. 14, a schematic diagram of the average vegetation biomass of the two over time is given, which mainly reflects the three totally differences between Gilad and its simplified model. The first point is the way in which the vegetation pattern reaches the steady state. The Gilad model tends to the steady state in an oscillatory manner with the passage of time, while the simplified model tends to the steady state in a monotonic manner. The second point is the average vegetation biomass after tending to steady state. Evidently, the final average biomass of the simplified model is higher than that of the Gilad model. The third point is the time spend for vegetation pattern to reach steady state. Compared with the simplified model, the Gilad model achieves steady state more swiftly and in less time.

Lastly, the spatial distribution of Gilad and its simplified model is compared and a sketch map of their spatial distribution is given in Fig. 15. This figure indicates that the periodicity of the spatial distribution of vegetation in the Gilad model is more regular compared with the simplified model (blue solid line in the figure). At the same time, we discover that the soil water content of the simplified model does not fluctuate significantly at different locations in space (Fig. 15b, orange dash line), which

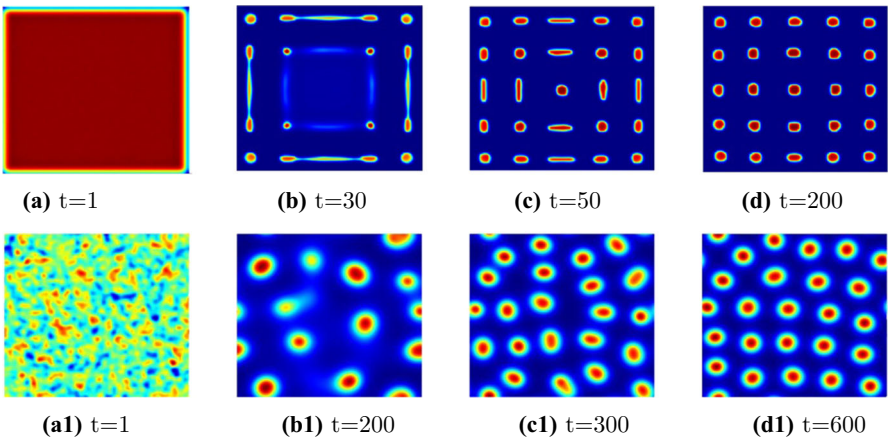

Fig. 13 Snapshot of spatial distribution of vegetation at different times, in which the first row is Gilad model and the second row is simplified model. With the evolution of time, the vegetation distribution of both of them presents a spot pattern structure. The red spots in the figure represent the vegetation with high biomass and the blue ones represent the vegetation with low biomass. Relevant parameter values involved can be obtained from Table 7

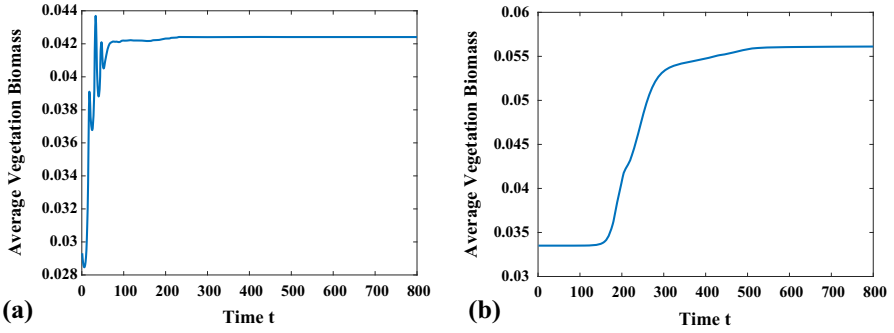

Fig. 14 Diagram of average vegetation biomass change over time, where **(a)** corresponds to Gilad model and **(b)** corresponds to simplified model. Over time, the average vegetation biomass tends to be stable and remains constant

is consistent with the assumptions we made when simplifying the model, that is, the areas with vegetation coverage (or high vegetation biomass) and without vegetation coverage (or low vegetation biomass) have the same soil water infiltration rates.

To summary, the comparative study between the Gilad model and its simplified model shows that the pattern structure of the two models are very similar. However, due to the difference between the two models, that is, the Gilad model considers the non-local effects of roots while the simplified model considers the local effects, which leads to the essential difference in the average biomass and spatial distribution of vegetation between the two models.

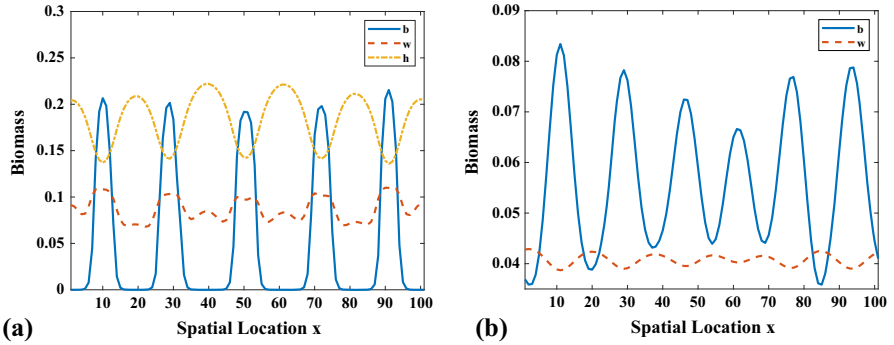

Fig. 15 Spatial distribution of Gilad model (**a**) and simplified model (**b**) after reaching steady state ($t = 1000$) in one-dimensional domain. The solid blue line represents the biomass of vegetation at different spatial locations x, the orange dash line represents the soil water content, and the yellow dotted line represents the surface water content

5 Discussion

In this paper, we mainly analyze the spatial dynamics based on the vegetation-water model proposed by Zelnik et al. (2015). Firstly, the existence and stability of the equilibrium points are analyzed, and the conditions of producing Turing pattern are studied according to Turing instability theory. Secondly, we derive the amplitude equation by using the method of multi-scale analysis, study the dynamical behavior of the system near the Turing bifurcation point by using the amplitude equation, and find out the accurate parameter range of the spatial model which can produce the pattern. Lastly, we reveal the influences of model parameters including water diffusion and shading effects on the pattern structures and biomass change of vegetation. Our results demonstrate that model parameters play a significant role in the spatial dynamics of vegetation growth.

The main principle of uptake–diffusion feedback is to use the root of vegetation to absorb water, resulting in concentration difference. In our system, the strength of uptake–diffusion feedback is reflected in parameter η (water absorption capacity of vegetation roots) and parameter δ_w (soil water diffusivity). The results show that the average biomass of vegetation gradually increases with the increase of water absorption capacity of vegetation roots, and tends to be stable with the passage of time (Fig. 10). At the same time, the pattern structure of vegetation also changed: spot pattern $\rightarrow$ labyrinth pattern $\rightarrow$ gap pattern (Fig. 9). We can find that the stronger the uptake–diffusion feedback, to a certain extent, can promote the growth of vegetation. However, with the increase of soil water diffusivity, the gap between patches becomes larger and larger (Fig. 7), that is, the distance between vegetation becomes larger and larger, which may lead to desertification.

In this work, we find the gradual regime shifts from The regime shifts refers to the uniform state to gap pattern. abrupt global transitions from one stable state to another alternative stable state due to small environmental changes or disturbances. Many studies have shown that this transition may also be gradual in a spatially expanding ecosystem. In a bistable range, there may be multiple stable hybrid states. Under small

disturbances, these stable hybrid states can be extended and merged to alternative stable states, which leads to this gradual regime shifts (Bel et al. 2012). In 2015, Zelnik et al. showed this kind of gradual regime shifts by studying the dynamics of Namibian fairy circle (Zelnik et al. 2015). In 2017, Zelnik et al. studied the existence and structure of the localized states in the model and the dynamical behavior nearby, and showed that the last step of desertification, that is, the transition from spot vegetation to bare soil, can only occur in a abrupt transition (Zelnik et al. 2017).

The pattern structure of vegetation is always a subject worthy of our study, which can reflect the elasticity and stability of ecosystem under external disturbance and environmental pressure. By studying the internal mechanism of vegetation pattern formation, which can help us protect vegetation and prevent land desertification to a certain extent. We all know that there are many factors affecting the pattern structure of vegetation, including natural factors (such as rainfall, temperature, light and other climatic factors) and human factors (such as deforestation, grazing and so on) (Yu et al. 2006; Wang et al. 2017; Baldi et al. 2013; Giesecke et al. 2017; Dumont et al. 2012; Raharimalala et al. 2010). At present, most of our models are based on the influence of rainfall on vegetation pattern. Research on the influence of other factors on vegetation pattern is relatively scarce (Kefi et al. 2008; Chen et al. 2021). Therefore, in order to better protect our ecological environment, it is still worth exploring how to establish a model that considers various influencing factors.

Acknowledgements The project is funded by the National Key Research and Development Program of China (Grant No. 2018YFE0109600), National Natural Science Foundation of China under Grant No. 42075029, Program for the Outstanding Innovative Teams (OIT) of Higher Learning Institutions of Shanxi, Natural Science Foundation of Shanxi Province (Grant No. 201801D221003), China Postdoctoral Science Foundation (Grant Nos. 2017M621110 and 2019T120199), and Outstanding Young Talents Support Plan of Shanxi province.

Declaration

Conflict of interest The authors have no competing interests to declare that are relevant to the content of this article.

Appendix A

In this section, we give the specific expressions of some parameter values involved in the process of deriving the amplitude equation.

$$
\begin{aligned}
N_1(x,y) &= -\lambda\eta^2 w_2^* x^4 - \lambda\eta x^4 y - m_{11}x^3 y - m_{11}w_2^* x^3 \\
&\quad -m_{12}x^2 y - m_{12}w_2^* x^2 + \frac{a_{11}+1}{w_2^*}xy, \\
N_2(x,y) &= -\lambda\eta^2 w_2^* x^3 - \lambda\eta x^3 y - m_{21}x^2 y - m_{21}w_2^* x^2 + \frac{a_{21}}{w_2^*}xy, \\
m_{11} &= \lambda\eta(4\eta b_2^* - \eta + 2), \\
m_{12} &= \lambda(6\eta^2 b_2^{*2} - 3\eta^2 b_2^* + 6\eta b_2^* - 2\eta + 1),
\end{aligned}
$$

$$m_{21} = \lambda\eta(3\eta b_2^* + 2),$$

$$h^2 = \begin{pmatrix} -m_{12}w_2^*x_1^2 + \dfrac{a_{11}+1}{w_2^*}x_1y_1 \\ -m_{21}w_2^*x_1^2 + \dfrac{a_{21}}{w_2^*}x_1y_1 \end{pmatrix},$$

$$h^3 = \begin{pmatrix} -m_{11}w_2^*x_1^3 - m_{12}x_1^2y_1 - 2m_{12}x_1x_2 + \dfrac{a_{11}+1}{w_2^*}(x_2y_1 + x_1y_2) \\ -\lambda\eta^2 w_2^*x_1^3 - m_{21}x_1^2y_1 - 2m_{21}x_1x_2 + \dfrac{a_{21}}{w_2^*}(x_2y_1 + x_1y_2) \end{pmatrix},$$

$$h_1 = -2m_{12}w_2^*l^2 + \frac{2(a_{11}+1)l}{w_2^*},$$

$$h_2 = -2m_{21}w_2^*l^2 + \frac{2a_{21}l}{w_2^*},$$

$$E_1 = \rho_1\left[lb_{11} + b_{12} - \frac{l}{\delta_w}(lb_{21} + b_{22})\right],$$

$$x_0 = \frac{1}{a_{11}^*a_{22}^* - a_{12}^*a_{21}^*}\left[-a_{22}^*\left(-2m_{12}w_2^*l^2 + \frac{2(a_{11}+1)l}{w_2^*}\right) + a_{12}^*\left(-\frac{2m_{21}w_2^*l^3}{\delta_w} + \frac{2a_{21}l^2}{\delta_w w_2^*}\right)\right],$$

$$y_0 = \frac{1}{a_{11}^*a_{22}^* - a_{12}^*a_{21}^*}\left[a_{21}^*\left(-2m_{12}w_2^*l^2 + \frac{2(a_{11}+1)l}{w_2^*}\right) - a_{11}^*\left(-\frac{2m_{21}w_2^*l^3}{\delta_w} + \frac{2a_{21}l^2}{\delta_w w_2^*}\right)\right],$$

$$x_{11} = \frac{1}{(a_{11}^* - 4k_T^2)(a_{22}^* - 4\delta_w k_T^2) - a_{12}^*a_{21}^*}\left[-(a_{22}^* - 4\delta_w k_T^2)\left(-2m_{12}w_2^*l^2 + \frac{2(a_{11}+1)l}{w_2^*}\right)\right.$$
$$\left. + a_{12}^*\left(-\frac{2m_{21}w_2^*l^3}{\delta_w} + \frac{2a_{21}l^2}{\delta_w w_2^*}\right)\right],$$

$$y_{11} = \frac{1}{(a_{11}^* - 4k_T^2)(a_{22}^* - 4\delta_w k_T^2) - a_{12}^*a_{21}^*}\left[a_{21}^*\left(-2m_{12}w_2^*l^2 + \frac{2(a_{11}+1)l}{w_2^*}\right)\right.$$
$$\left. - (a_{11}^* - 4k_T^2)\left(-\frac{2m_{21}w_2^*l^3}{\delta_w} + \frac{2a_{21}l^2}{\delta_w w_2^*}\right)\right],$$

$$x_* = \frac{1}{(a_{11}^* - 3k_T^2)(a_{22}^* - 3\delta_w k_T^2) - a_{12}^*a_{21}^*}\left[-(a_{22}^* - 3\delta_w k_T^2)\left(-2m_{12}w_2^*l^2 + \frac{2(a_{11}+1)l}{w_2^*}\right)\right.$$
$$\left. + a_{12}^*\left(-\frac{2m_{21}w^*l^3}{\delta_w} + \frac{2a_{21}l^2}{\delta_w w_2^*}\right)\right],$$

$$y_* = \frac{1}{(a_{11}^* - 3k_T^2)(a_{22}^* - 3\delta_w k_T^2) - a_{12}^*a_{21}^*}\left[a_{21}^*\left(-2m_{12}w_2^*l^2 + \frac{2(a_{11}+1)l}{w_2^*}\right)\right.$$
$$\left. - (a_{11}^* - 3k_T^2)\left(-\frac{2m_{21}w_2^*l^3}{\delta_w} + \frac{2a_{21}l^2}{\delta_w w_2^*}\right)\right],$$

$$\begin{pmatrix} H_x^1 \\ H_y^1 \end{pmatrix} = \begin{pmatrix} l\dfrac{\partial Y_1}{\partial T_1} \\ \dfrac{\partial Y_1}{\partial T_1} \end{pmatrix} + \begin{pmatrix} l\dfrac{\partial W_1}{\partial T_2} \\ \dfrac{\partial W_1}{\partial T_2} \end{pmatrix} - \rho_1 \begin{pmatrix} lb_{11}Y_1 + b_{12}Y_1 \\ lb_{21}Y_1 + b_{22}Y_1 \end{pmatrix} - \rho_2 \begin{pmatrix} lb_{11}W_1 + b_{12}W_1 \\ lb_{21}W_1 + b_{22}W_1 \end{pmatrix}$$
$$+ \begin{pmatrix} M_{11}|W_1|^2 + M_{12}(|W_2|^2 + |W_2|^2) \\ M_{21}|W_1|^2 + M_{22}(|W_2|^2 + |W_2|^2) \end{pmatrix} W_1 - \begin{pmatrix} h_1 \\ h_2 \end{pmatrix} (\bar{W}_2\bar{Y}_3 + \bar{W}_3\bar{Y}_2),$$

$$M_{11} = 3m_{11}w_2^*l^3 + 3m_{12}l^2 + \left(2m_{12}w_2^*l - \frac{a_{11}+1}{w_2^*}\right)(x_0 + x_{11}) - \frac{(a_{11}+1)l}{w_2^*}(y_0 + y_{11}),$$
$$M_{12} = 6m_{11}w_2^*l^3 + 6m_{12}l^2 + \left(2m_{12}w_2^*l - \frac{a_{11}+1}{w_2^*}\right)(x_0 + x_*) - \frac{(a_{11}+1)l}{w_2^*}(y_0 + y_*),$$
$$M_{21} = 3\lambda\eta^2 w_2^*l^3 + 3m_{21}l^2 + \left(2m_{21}w_2^*l - \frac{a_{21}}{w_2^*}\right)(x_0 + x_{11}) - \frac{a_{21}l}{w_2^*}(y_0 + y_{11}),$$
$$M_{22} = 6\lambda\eta^2 w_2^*l^3 + 6m_{21}l^2 + \left(2m_{21}w_2^*l - \frac{a_{21}}{w_2^*}\right)(x_0 + x_*) - \frac{a_{21}l}{w_2^*}(y_0 + y_*).$$

References

Baldi G, Verón SR, Jobbágy EG (2013) The imprint of humans on landscape patterns and vegetation functioning in the dry subtropics. Glob Change Biol 19:441–458. https://doi.org/10.1111/gcb.12060

Barbier N, Couteron P, Lejoly J, Deblauwe V, Lejeune O (2006) Self-organized vegetation patterning as a fingerprint of climate and human impact on semi-arid ecosystems. J Ecol 94:537–547. https://doi.org/10.1111/j.1365-2745.2006.01126.x

Bel G, Hagberg A, Meron E (2012) Gradual regime shifts in spatially extended ecosystems. Thyroid Res 5:591–604. https://doi.org/10.1007/s12080-011-0149-6

Borgogno F, D'Odorico P, Laio F, Ridolfi L (2009) Mathematical models of vegetation pattern formation in ecohydrology. Rev Geophys 47:1–36. https://doi.org/10.1029/2007RG000256

Chen Z, Wu Y-P, Feng G-L, Qian Z-H, Sun G-Q (2021) Effects of global warming on pattern dynamics of vegetation: Wuwei in china as a case. Appl Math Comput 390:125666. https://doi.org/10.1016/j.amc.2020.125666

Cross M, Greenside H (2009) Pattern formation and dynamics in nonequilibrium systems. Cambridge University Press, Cambridge

Dumont B, Rossignol N, Loucougaray G, Carrère P, Chadoeuf J, Fleurance G, Bonis A, Farruggia A, Gaucherand S, Ginane C et al (2012) When does grazing generate stable vegetation patterns in temperate pastures? Agric Ecosyst Environ 153:50–56. https://doi.org/10.1016/j.agee.2012.03.003

Gallagher RV, Allen S, Wright IJ (2019) Safety margins and adaptive capacity of vegetation to climate change. Sci Rep 9:1–11. https://doi.org/10.1038/s41598-019-44483-x

Garfinkel A, Tintut Y, Petrasek D, Boström K, Demer LL (2004) Pattern formation by vascular mesenchymal cells. Proc Natl Acad Sci 101:9247–9250. https://doi.org/10.1073/pnas.0308436101

Giesecke T, Brewer S, Finsinger W, Leydet M, Bradshaw RH (2017) Patterns and dynamics of European vegetation change over the last 15,000 years. J Biogeogr 44:1441–1456. https://doi.org/10.1111/jbi.12974

Gilad E, von Hardenberg J, Provenzale A, Shachak M, Meron E (2004) Ecosystem engineers: from pattern formation to habitat creation. Phys Rev Lett 93:098105. https://doi.org/10.1103/PhysRevLett.93.098105

Gilad E, von Hardenberg J, Provenzale A, Shachak M, Meron E (2007) A mathematical model of plants as ecosystem engineers. J Theor Biol 244:680–691. https://doi.org/10.1016/j.jtbi.2006.08.006

Gommers CM, Visser EJ, St Onge KR, Voesenek LA, Pierik R (2013) Shade tolerance: when growing tall is not an option. Trends Plant Sci 18:65–71. https://doi.org/10.1016/j.tplants.2012.09.008
HilleRisLambers R, Rietkerk M, van den Bosch F, Prins HH, de Kroon H (2001) Vegetation formation in semi-arid grazing systems. Ecology 82:50–61. https://doi.org/10.1890/0012-9658(2001)082
Jones CG, Lawton JH, Shachak M (1994) Organisms as ecosystem engineers. Oikos 69:373–386. https://doi.org/10.1007/978-1-4612-4018-1_14
Kéfi S, Rietkerk M, Alados CL, Pueyo Y, Papanastasis VP, ElAich A, De Ruiter PC (2007) Spatial vegetation patterns and imminent desertification inmediterranean arid ecosystems. Nature 449:213–217. https://doi.org/10.1038/nature06111
Kefi S, Rietkerk M, Katul GG (2008) Vegetation pattern shift as a result of rising atmospheric co_2 in arid ecosystems. Theor Popul Biol 74:332–344. https://doi.org/10.1016/j.tpb.2008.09.004
Kinast S, Zelnik YR, Bel G, Meron E (2014) Interplay between Turing mechanisms can increase pattern diversity. Phys Rev Lett 112:078701. https://doi.org/10.1103/PhysRevLett.112.078701
Klausmeier CA (1999) Regular and irregular patterns in semiarid vegetation. Science 284:1826–1828. https://doi.org/10.1126/science.284.5421.1826
Lejeune O, Tlidi M, Lefever R (2004) Vegetation spots and stripes: dissipative structures in arid landscapes. Int J Quantum Chem 98:261–271. https://doi.org/10.1002/qua.10878
Lemordant L, Gentine P, Swann AS, Cook BI, Scheff J (2018) Critical impact of vegetation physiology on the continental hydrologic cycle in response to increasing co_2. Proc Natl Acad Sci 115:4093–4098. https://doi.org/10.1073/pnas.1720712115
Li J, Sun G-Q, Guo Z-G (2022a) Bifurcation analysis of an extended Klausmeier–Gray–Scott model with infiltration delay. Stud Appl Math 148:1519–1542. https://doi.org/10.1111/sapm.12482
Li J, Sun G-Q, Jin Z (2022b) Interactions of time delay and spatial diffusion induce the periodic oscillation of the vegetation system. Discrete Continu Dyn Syst B 27:2147–2172. https://doi.org/10.3934/dcdsb.2021127
Loreau M, Naeem S, Inchausti P, Bengtsson J, Grime JP, Hector A, Hooper D, Huston M, Raffaelli D, Schmid B et al (2001) Biodiversity and ecosystem functioning: current knowledge and future challenges. Science 294:804–808. https://doi.org/10.1126/science.1064088
Meron E (2011) Modeling dryland landscapes. Math Model Nat Phenom 6:163–187. https://doi.org/10.1051/mmnp/20116109
Meron E (2012) Pattern-formation approach to modelling spatially extended ecosystems. Ecol Model 234:70–82. https://doi.org/10.1016/j.ecolmodel.2011.05.035
Meron E (2018) From patterns to function in living systems: dryland ecosystems as a case study. Annu Rev Condens Matter Phys 9:79–103. https://doi.org/10.1146/annurev-conmatphys-033117-053959
Meron E, Gilad E, Von Hardenberg J, Shachak M, Zarmi Y (2004) Vegetation patterns along a rainfall gradient. Chaos Solitons Fractals 19:367–376. https://doi.org/10.1016/S0960-0779(03)00049-3
Ouyang Q (2000) Pattern formation in reaction–diffusion systems, Shanghai Sci-Tech Education Publishing (**in Chinese**)
Raharimalala O, Buttler A, Ramohavelo CD, Razanaka S, Sorg J-P, Gobat J-M (2010) Soil-vegetation patterns in secondary slash and burn successions in central Menabe, Madagascar. Agric Ecosyst Environ 139:150–158. https://doi.org/10.1016/j.agee.2010.07.013
Rietkerk M, Van de Koppel J (2008) Regular pattern formation in real ecosystems. Trends Ecol Evol 23:169–175. https://doi.org/10.1016/j.tree.2007.10.013
Rietkerk M, Boerlijst MC, van Langevelde F, HilleRisLambers R, de Koppel KL, Prins HH, de Roos AM (2002) Self-organization of vegetation in arid ecosystems. Am Nat 160:524–530. https://doi.org/10.1086/342078
Rietkerk M, Dekker SC, De Ruiter PC, van de Koppel J (2004) Self-organized patchiness and catastrophic shifts in ecosystems. Science 47:1926–1929. https://doi.org/10.1126/science.1101867
Sherratt JA (2005) An analysis of vegetation stripe formation in semi-arid landscapes. J Math Biol 51:183–197. https://doi.org/10.1007/s00285-005-0319-5
Sherratt JA (2015) Using wavelength and slope to infer the historical origin of semi-arid vegetation bands. Proc Natl Acad Sci USA 112:4202–4207. https://doi.org/10.1073/pnas.1420171112
Sherratt JA, Lord GJ (2007) Nonlinear dynamics and pattern bifurcations in a model for vegetation stripes in semi-arid environments. Theor Popul Biol 71:1–11. https://doi.org/10.1016/j.tpb.2006.07.009Get
Sherratt JA, Synodinos AD (2012) Vegetation patterns and desertification waves in semi-arid environments: mathematical models based on local facilitation in plants. Discrete Continu Dyn Syst Ser B 17:2815–2827. https://doi.org/10.3934/dcdsb.2012.17.2815

Sun G-Q (2016) Mathematical modeling of population dynamics with Allee effect. Nonlinear Dyn 85:1–12. https://doi.org/10.1007/s11071-016-2671-y
Sun G-Q, Wang C-H, Chang L-L, Wu Y-P, Li L, Jin Z (2018) Effects of feedback regulation on vegetation patterns in semi-arid environments. Appl Math Model 61:200–215. https://doi.org/10.1016/j.apm.2018.04.010
Sun G-Q, Zhang H-T, Song Y-L, Li L, Jin Z (2022) Dynamic analysis of a plant–water model with spatial diffusion. J Differ Equ 329:395–430. https://doi.org/10.1016/j.jde.2022.05.009
Turing AM (1952) The chemical basis of morphogenesis. Bull Math Biol 237:37–72. https://doi.org/10.1007/BF02459572
von Hardenberg J, Meron E, Shachak M, Zarmi Y (2001) Diversity of vegetation patterns and desertification. Phys Rev Lett 87:198101. https://doi.org/10.1103/PhysRevLett.87.198101
Wang X, Gao Q, Wang C, Yu M (2017) Spatiotemporal patterns of vegetation phenology change and relationships with climate in the two transects of east China. Global Ecol Conserv 10:206–219. https://doi.org/10.1016/j.gecco.2017.01.010
Yachi S, Loreau M (1999) Biodiversity and ecosystem productivity in a fluctuating environment: the insurance hypothesis. Proc Natl Acad Sci USA 96:1463–1468. https://doi.org/10.1073/pnas.96.4.1463
Yu L, Cao M, Li K (2006) Climate-induced changes in the vegetation pattern of china in the 21st century. Ecol Res 21:912–919. https://doi.org/10.1007/s11284-006-0042-8
Zelnik YR, Kinast S, Yizhaq H, Bel G, Meron E (2013) Regime shifts in models of dryland vegetation. Philos Trans 371:0358. https://doi.org/10.1098/rsta.2012.0358
Zelnik YR, Meron E, Bel G (2015) Gradual regime shifts in fairy circles. Proc Natl Acad Sci 112:12327–12331. https://doi.org/10.1073/pnas.1504289112
Zelnik YR, Meron E, Bel G (2016) Localized states qualitatively change the response of ecosystems to varying conditions and local disturbances. Ecol Complex 25:26–34. https://doi.org/10.1016/j.ecocom.2015.11.004
Zelnik YR, Uecker H, Feudel U, Meron E (2017) Desertification by front propagation? J Theor Biol 418:27–35. https://doi.org/10.1016/j.jtbi.2017.01.029
Zhang X-C, Sun G-Q, Jin Z (2012) Spatial dynamics in a predator-prey model with Beddington–Deangelis functional response. Phys Rev E 85:021924. https://doi.org/10.1103/PhysRevE.85.021924